MgPd$_2$Sb: A Mg-based Heusler-type superconductor

M. J. Winiarski [1,2,*] G. Kuderowicz,[3] K. Górnicka,[1,2] L. S. Litzbarski,[1,2] K. Stolecka,[1]
B. Wiendlocha [3] R. J. Cava,[4] and T. Klimczuk [1,2,†]

[1]*Faculty of Applied Physics and Mathematics, Gdansk University of Technology,*
ulica Narutowicza 11/12, 80-233 Gdansk, Poland
[2]*Advanced Materials Centre, Gdansk University of Technology, ulica Narutowicza 11/12, 80-233 Gdańsk, Poland*
[3]*Faculty of Physics and Applied Computer Science, AGH University of Science and Technology,*
Aleja Mickiewicza 30, 30-059 Kraków, Poland
[4]*Department of Chemistry, Princeton University, Princeton, New Jersey 08544, USA*

We report the synthesis and physical properties of a full Heusler compound, MgPd$_2$Sb, which we found to show superconductivity below $T_c = 2.2$ K. MgPd$_2$Sb was obtained by a two-step solid-state reaction method and its purity and cubic crystal structure [Fm-$3m$, $a = 6.4523(1)$ Å] were confirmed by powder x-ray diffraction. Normal and superconducting states were studied by electrical resistivity, magnetic susceptibility, and heat capacity measurements. The results show that MgPd$_2$Sb is a type-II, weak coupling superconductor ($\lambda_{e\text{-}p} = 0.53$). The observed pressure dependence of T_c ($\Delta T_c/p \approx -0.23$ K/GPa) is one of the strongest reported for a superconducting Heusler compound. The electronic structure, phonons, and electron-phonon coupling in MgPd$_2$Sb were theoretically investigated. The obtained results are in agreement with the experiment, confirming the electron-phonon coupling mechanism of superconductivity. We compare the superconducting parameters to those of all reported Heusler-type superconductors.

I. INTRODUCTION

Heusler phases constitute a large family of intermetallic compounds with hundreds of members [1,2]. The prototype member MnCu$_2$Al was discovered by Heusler in 1903 and was the first known ferromagnetic material that was not composed of elements showing ferromagnetism in their pristine form [3]. The cubic MnCu$_2$Al-type structure (space group No. 225, Fm-$3m$) can be considered as composed of a NaCl-type sublattice of AB (CuAl in the prototypic phase) with C (Mn) atoms filling all its tetrahedral voids (Fig. 1). If only half of the voids are filled in an ordered manner, the so-called half-Heusler noncentrosymmetric (space group No. 214, F-$43m$) structure results. In general, in most of the known Heusler compounds the A site is occupied by an electropositive element (rare-earth metals, early transition elements), B by an electronegative p-block element (groups 13–15 of the periodic table), and the C site by a late transition metal (groups 9–11).

Both Heusler and half-Heusler phases have attracted significant research interest, due to their chemical versatility leading to a plethora of ground states and properties, including superconductivity [4–8], topologically nontrivial states [9–13], and half-metallic ferromagnetism [14–18]. Many of the properties can be tuned by chemical substitution [16,19–21] or mechanical strain [22,23], and the relative chemical and structural simplicity allows the growth of Heusler phase based superstructures and nanosized (thin films, nanowires) forms [24,25].

Only 34 full Heusler-type superconductors are reported, with critical temperatures reaching up to $T_c \approx 5$ K (YPd$_2$Sn) [4,5], all of them featuring rare-earth elements or early transition metals (Zr, Hf, Nb) at the A site and most of them having Pd at the C site [5,8]. A list of selected superconducting parameters for all members of this family of superconductors can be found in Table I.

Based on a previously observed relation between the superconducting T_c and the valence electron count (VEC), showing a maximum around VEC $= 27$ [5], we have selected MgPd$_2$Sb as a candidate superconductor. The crystal structure of the compound was reported by Graf *et al.* [26] and it was predicted to be thermodynamically stable based on high-throughput electronic structure calculations in the Materials Project database [27,28]. Thanks to their simple crystal structure, total energies of numerous hypothetical Heusler-type compounds were calculated, which allows prediction of their thermodynamic stability. It is worth noting that in the Open Quantum Materials Database, OQMD, the Heusler phase of MgPd$_2$Sb (id: 468110) is predicted to be slightly less stable than tetragonal (id: 1014836) and orthorhombic (id: 1015910) variants of the same composition, with a minute energy difference of ca. 2 meV/atom [29,30]). In this paper we report superconductivity in MgPd$_2$Sb and discuss its properties in the context of the Pd-based Heusler superconductor family. Our finding supports the applicability of the VEC-T_c relationship of Heusler superconductors.

II. MATERIALS AND METHODS

Polycrystalline samples of MgPd$_2$Sb were synthesized via a two-step solid-state reaction. First a precursor compound,

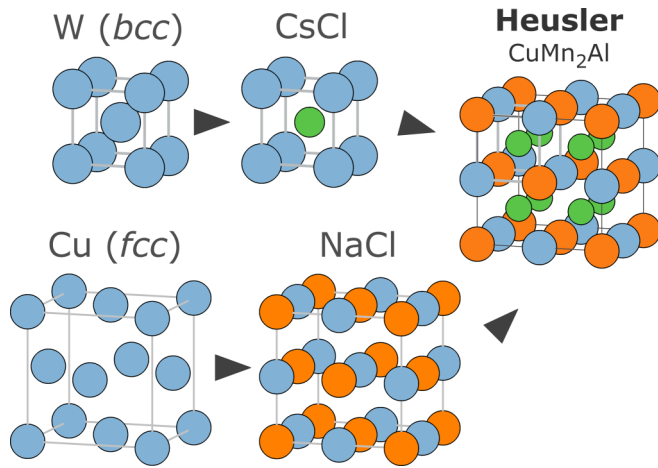*michal.winiarski@pg.edu.pl
†tomasz.klimczuk@pg.edu.pl

FIG. 1. Relationship between the (full) Heusler and simple close-packed structures. The Heusler structure (e.g., of CuMn$_2$Al) can be viewed as an ordered superstructure of CsCl-type structure, which itself is an ordered variant of a simple bcc lattice as found in elemental W. Alternatively the Heusler structure can be obtained by filling tetrahedral voids of the NaCl-type lattice, which is an ordered variant of the fcc cell, represented, e.g., by metallic Cu. In half-Heusler phases (MgAgAs type) only every other tetrahedral void of the NaCl substructure is filled, resulting in a noncentrosymmetric structure.

PdSb, was synthesized by reacting Pd and Sb powders pressed into a pellet and annealed at 800 °C for 5 h, sealed in an evacuated silica ampoule. Stoichiometric amounts of Pd and PdSb powders with a slight (2%) excess of metallic Mg flakes were mixed, pressed into pellets, wrapped with Ta foil, and sealed in evacuated silica ampoules, backfilled with Ar to reduce the Mg evaporation during annealing. Ampoules were subsequently slowly heated (50 °C/h) to 600 °C, kept for 5 h, and furnace cooled to room temperature. After the first annealing the resulting pellets were ground, re-pressed, and annealed at 700 °C for 5 h, resulting in relatively hard, dense samples. It is worth noting that similar to other Mg-based superconductors, e.g., Mg$_{10}$Ir$_{19}$B$_{16}$ [31] and MgCNi$_3$ [32], the Mg excess is important for observing superconductivity. However, we found that if more than 5%–10% Mg surplus is taken, superconductivity is not observed and the full Heusler MgPd$_2$Sb decomposes to a half-Heusler MgPdSb structure.

Analysis of the crystal structure of the synthesized samples was done by means of powder x-ray diffraction (PXRD) using a Bruker D2 Phaser diffractometer equipped with solid-state detector, using Cu K_α radiation. XRD patterns were processed by means of the Rietveld refinement method using the FULL-PROF software package [33].

Measurements of physical properties were performed using a Quantum Design (QD) Physical Properties Measurement System (PPMS). For magnetization the vibrating sample magnetometer (VSM) option was used. Heat capacity was measured employing the standard semiadiabatic pulse technique in the ^{3}He PPMS setup. The sample was attached to the measuring stage using Apiezon N grease to ensure good thermal contact. Resistivity measurements were performed using a four-probe technique with thin Pt wires ($d = 50 \, \mu$m) mounted using silver epoxy to the surface of a rectangular bar cut out of the sample pellet. High-pressure resistivity was

measured using a Quantum Design piston-cylinder type pressure cell. Idemitsu Kosan Co. Daphne 7373 oil was applied as the pressure transmitting medium.

Following the experimental study, electronic structure, the phonons, and electron-phonon coupling in MgPd$_2$Sb were theoretically investigated. Calculations were performed with the density functional theory implemented in QUANTUM ESPRESSO [34,35] which uses the plane-wave pseudopotential method. Ultrasoft pseudopotentials were chosen [36] with the Perdew-Burke-Ernzerhof generalized gradient approximation exchange-correlation functional [37]. Computation details are 60 Ry wave-function energy cutoff, 600 Ry charge density cutoff, 24^3 k-point Monkhorst-Pack grid for the electronic structure and 8^3 q-point grid for the force constant matrix evaluation. The role of spin-orbit coupling (SOC) was checked by including spin-orbit coupling and relativistic versions of pseudopotentials of Pd and Sb (replacing scalar Mg pseudopotential with the relativistic one had negligible effect) in the electronic structure and few selected q vectors in phonon frequency calculations.

The unit cell was relaxed with the Broyden-Fletcher-Goldfarb-Shanno algorithm. Atomic positions are fixed by the symmetry, and hence only the lattice constant was varied. The calculated value for a, 6.548 Å, is close to the one calculated by the Materials Project [27] (6.553 Å), slightly larger than the experimental one (see below). Then, the electronic bands, density of states (DOS), and Fermi surface were calculated. Phonons and their linewidths were calculated with the density functional perturbation theory [38]. Superconductivity with electron-phonon coupling was analyzed using Eliashberg functions, calculated from the phonon linewidths.

III. RESULTS AND DISCUSSION

Figure 2 shows the room temperature powder XRD pattern of MgPd$_2$Sb with a Rietveld fit. Resulting unit cell and structural parameters are gathered in Table II. The refined unit cell parameter $a = 6.452$ Å is in agreement with the above-mentioned computed values. No tetragonal or orthorhombic distortion, as predicted by OQMD calculations [29,30], was observed at room temperature within the experimental resolution of PXRD.

The temperature-dependent electrical resistivity of MgPd$_2$Sb [Fig. 3(a)] shows a typical metallic character with residual resistivity ratio RRR ≈ 1.9, a value similar to that observed in other Heusler superconductors [4,5]. A drop to zero is observed with an onset at ca. $T = 2.2$ K in zero magnetic field [Fig. 3(b)]. The transition is slightly broad ($\Delta T_c \approx 0.15$ K, $\Delta T_c/T_c \approx 7\%$), which may result from the presence of possible structural disorder. This suggests the presence of the antisite disorder commonly observed in Heusler compounds [4].

Figure 4 shows the temperature dependence of the upper critical field as extracted from the resistivity measurement. A linear fit to the data yields the coefficient $d\mu_0 H_{c2}/dT = -144(2)$ mT/K and the zero-field $T_c = 2.1$ K. Using the Werthamer-Helfand-Hohenberg relation [39,40]: the upper critical field $\mu_0 H_{c2}(0)$ can be estimated from

$$\mu_0 H_{c2}(0) = -A T_c \left| \frac{d\mu_0 H_{c2}(T)}{dT} \right|_{T \to T_c}.$$

TABLE I. Normal- and superconducting-state properties of Heusler superconductors. Unless noted otherwise the pressure dependence coefficient is taken from Ref. [51] and all other parameters from Ref. [5] and references therein.

Property	T_c (K)	Θ_D(K)	γ (mJ mol^{-1} K^{-2})	$\Delta C_p/\gamma T_c$	λ_{e-p}	$\mu_0 H_{c2}(0)$(T)	ξ_{GL} (nm)	$\Delta T_c/P$(K/GPa)
				VEC = 16				
LiGa$_2$Rh	2.4 [52]	320 [52]	4.7 [52]	1.48 [52]	0.52 [52]	0.31 [52]	33 [52]	–
				VEC = 25				
LiPd$_2$Ge	1.96 [44]	194(3) [44]	5.8(1) [44]	1.38 [44]	0.56 [44]	[a]	–	–
				VEC = 26				
YPd$_2$In	0.85	–	–	–	–	–	–	–
LuPt$_2$In[b]	0.45 [50]	190 [50]	–	–	0.43[c]	–	–	–
				VEC = 27				
MgPd$_2$Sb	2.1	250(16)	4.9(3)	1.20	0.53	0.194(3)	41.2(3)	−0.23(2)
ZrPd$_2$Al	3.4	189(1)	9.0(1)	1.02	0.65	2.82	11	–
HfPd$_2$Al	3.66	182(3)	7.9(3)	1.50	0.68	1.81	13	−0.13(1) [42]
ZrPd$_2$In	2.19	236(5)	10.9(2)	–	0.55	0.63	23	–
HfPd$_2$In	2.86	243(5)	8.5(2)	1.72	0.58	1.00	18	–
ScPd$_2$Sn	2.0	277(1)	6.6(2)	–	0.52	0.26	36	−0.15(10)
YPd$_2$Sn	4.7	210(4)	9.2(2)	1.73	0.70	0.90	19	−0.226(21)
LuPd$_2$Sn	2.8	246(2)	7.4(1)	1.45	0.58	0.45	27	−0.168(7)
ScPd$_2$Pb	2.4	–	–	–	–	–	–	–
YPd$_2$Pb	2.3	198 [53]	–	–	0.58[c]			−0.193(9)
LuPd$_2$Pb	2.4	–	–	–	–	–	–	–
ErPd$_2$Sn[d]	1.17	–	–	–	–	–	–	–
TmPd$_2$Sn	2.82	120[e] [53]	–	–	0.72[c]			–
YbPd$_2$Sn[d]	2.46	118[e] [53]	6.0 [54]	–	0.69[c]			−0.193(9)
TmPd$_2$Pb	2.1	–	–	–	–	–	–	−0.262(9)
YbPd$_2$Pb	2.8	–	–	–	–	–	–	–
ZrNi$_2$Al	1.38	278(2) [55]	13.7(2) [55]	–	0.48[c]	–	–	–
HfNi$_2$Al	0.74	288(1) [55]	10.9(2) [55]	–	0.43[c]	–	–	–
ZrNi$_2$Ga	2.85 [56]	300 [56]	17.3 [56]	1.41 [56]	0.55 [56]	1.48 [56]	15[f]	–
HfNi$_2$Ga	1.12	–	–	–	–	–	–	–
ScPdAuAl	3.0 [49,57]	–	–	–	–	–	–	–
ScPtAuIn	0.96 [49]	–	–	–	–	–	–	–
YPdAuIn	2.6 [49]	–	–	–	–	–	–	–
				VEC = 28				
ScAu$_2$Al	4.4	–	–	–	–	–	–	–
NbNi$_2$Al	2.15	280 [58]	8.0 [58]	1.8 [58]	0.52 [58]	1.35 [58]	16[f]	–
NbNi$_2$Ga	1.54	240 [58]	6.5 [58]	–	0.50 [58]	0.60 [58]	23[f]	–
ScAu$_2$In	3	–	–	–	–	–	–	–
YAu$_2$In	1.74	–	–	–	–	–	–	–
YPd$_2$Sb	0.85	–	–	–	–	–	–	–
				VEC = 29				
NbNi$_2$Sn	2.90	206 [58]	4.0 [58]	1.6 [58]	0.61 [58]	0.63 [58]	23[f]	–

[a]According to our knowledge LiPd$_2$Ge is the only type-I superconductor in the Heusler family ($\mu_0 H_c = 34.2$ mT) [44].

[b]Superconductivity coexistent with a charge density wave distortion.

[c]λ_{e-p} was not reported in the literature and was obtained using the McMillan equation based on the reported values of Debye temperature and T_c.

[d]Superconductivity coexistent with magnetic order.

[e]Extrapolated Θ_D values, likely underestimated.

[f]ξ_{GL} calculated based on the reported value of the upper critical field.

Numbers in parentheses are uncertainties of the least significant digits (where available).

Assuming the dirty limit value of the prefactor A (0.69) and $T_c = 2.1$ K the $\mu_0 H_{c2}(0) = 194$ mT. The superconducting coherence length can be calculated using the extrapolated value of the upper critical field via
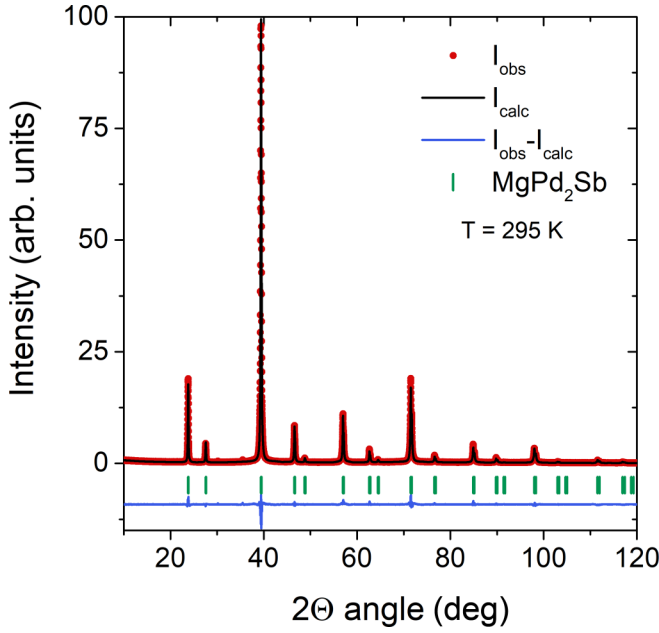
$$\xi_{GL} = \sqrt{\frac{\phi_0}{2\pi\mu_0 H_{c2}}},$$

FIG. 2. Rietveld fit (black line) to the room temperature powder XRD pattern of MgPd$_2$Sb (red points). Blue line shows the difference between observed and model intensities. Green ticks mark the expected positions of Bragg reflections.
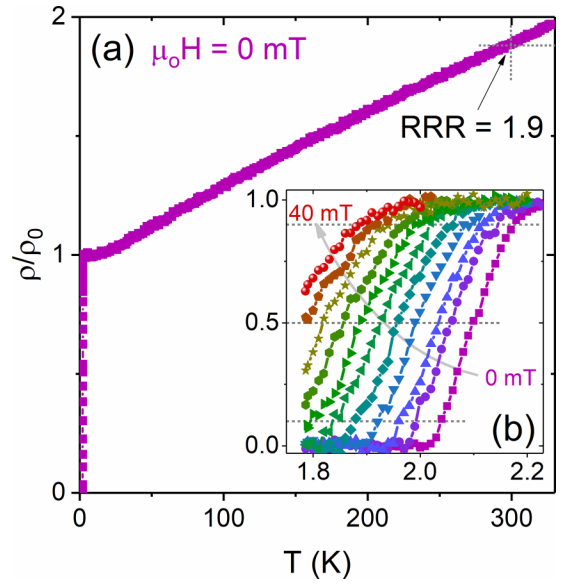

FIG. 3. Normalized resistivity of MgPd$_2$Sb [$\rho(T)$ divided by residual resistivity ρ_0]. Main figure shows $\rho(T)/\rho_0$ at zero field in the temperature range of 2–330 K. Inset: low-temperature resistivity in applied magnetic fields $\mu_0 H$ from 0 to 40 mT (5 mT spacing). Three horizontal dotted lines are drawn at 90%, 50%, and 10% of the residual resistivity ρ_0.

where ϕ_0 is the quantum of magnetic flux. This gives $\xi_{GL} = 412$ Å.

To further characterize the superconducting state of MgPd$_2$Sb, we have performed measurements of the dc magnetization vs temperature, as well as vs magnetic field. Temperature-dependent dc magnetic susceptibility measured at an applied magnetic field of $H = 10$ Oe is shown in Fig. 5(a). At $T \approx 2.15$ K the onset of transition to the Meissner state is observed, with the critical temperature $T_c = 2.0$ K. The difference between zero field cooled and field-cooled curves results from magnetic flux pinning between polycrystalline grains. Panel (b) presents the hysteretic $M(H)$ loop

TABLE II. Unit cell parameters and isotropic thermal displacement factors derived from Rietveld fit to room temperature powder XRD data. Numbers in parentheses are statistical standard uncertainties of least significant digits.

Formula unit	MgPd$_2$Sb
Z	4
Space group	Fm-$3m$ (No. 225)
Unit cell parameter a (Å)	6.4523(1)
Cell volume V (Å^3)	268.62(1)
Calculated density ρ (g/cm^3)	8.87
Reliability factors for	$R_p = 8.73\%$
Rietveld model:	$R_{wp} = 10.3\%$
	$R_{exp} = 4.92\%$
	$\chi^2 = 4.41$
Atomic positions	Isotropic thermal factors B_{iso} (Å^2)
Mg ($4a$) (0 0 0)	2.39(6)
Pd ($8c$) ($\frac{1}{4}$ $\frac{1}{4}$ $\frac{1}{4}$)	3.31(2)
Sb ($4b$) (0 0 $\frac{1}{2}$)	2.57(2)

measured at 1.7 K. The shape of the $M(H)$ curves is suggestive of type-II superconductivity.

The specific heat $C_p(T)$ between 0.5 and 3 K measured in zero applied magnetic field is shown in Fig. 6. A lambda-shaped anomaly is seen with the transition temperature $T = 1.95$ K which was obtained by using an equal entropy construction [Fig. 6(a)]. The $C_p(T)$ data above the transition
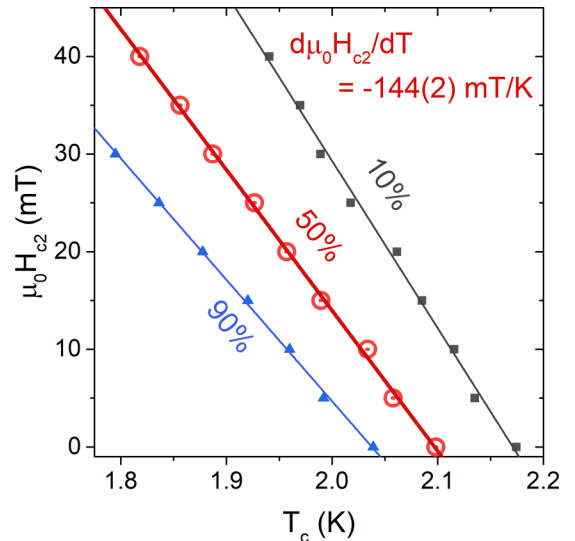

FIG. 4. Temperature dependence of the upper critical field as extracted from temperature-dependent resistivity measurements at applied magnetic fields [see Fig. 3(b)] using 10%, 50%, and 90% resistivity drop criterion (gray, red, and blue points, respectively). Thick red line is a linear fit to the 50% data, yielding $d\mu_0 H_{c2}/dT = -144(2)$ mT/K. The thin gray and blue lines are guides for the eyes.
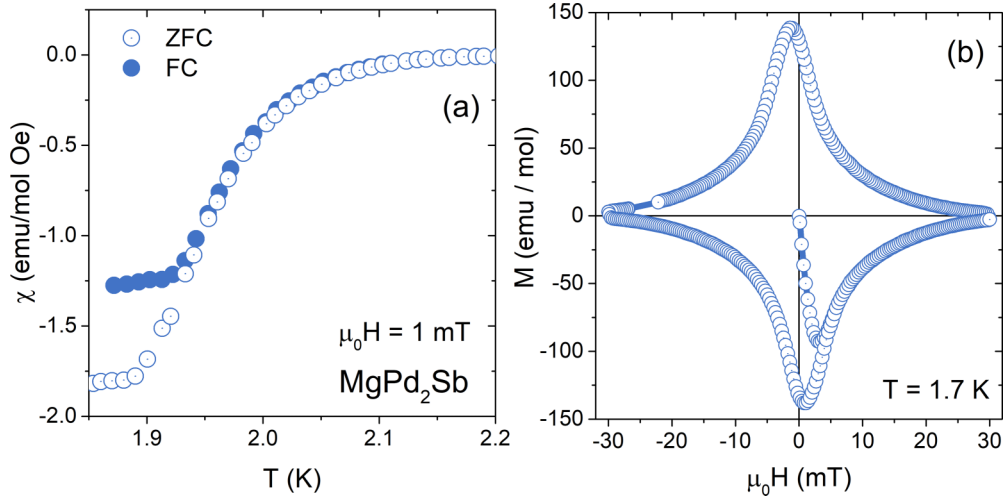
FIG. 5. (a) Zero-field cooling (ZFC) and field-cooling (FC) dc molar magnetic susceptibility of MgPd$_2$Sb in an applied field of $\mu_0 H =$ 1 mT showing a transition to the Meissner state. (b) Hysteresis loop of the molar magnetization $M(H)$ at 1.7 K.

temperature was fitted with the formula

$$\frac{C_p}{T} = \gamma + \beta_3 T^2 + \beta_5 T^4,$$

where γ is the Sommerfeld coefficient and the β parameters describe the phonon heat capacity contribution. The β_5 contribution is added to model a deviation from linearity of the C_p/T vs T^2 relation. The fit, shown by a solid line in Fig. 6(b), yields $\gamma = 4.9(3)$ mJ mol^{-1} K^{-2}, $\beta_3 = 0.49(9)$ mJ mol^{-1} K^{-4}, and $\beta_5 = 0.031(6)$ mJ mol^{-1} K^{-6}. The β_3 coefficient is related to the Debye temperature via

$$\Theta_D = \sqrt[3]{\frac{12\pi^4 nR}{5\beta_3}}.$$

The estimated $\Theta_D = 250$ K falls within the range observed for other Heusler superconductors (180–240 K in MPd$_2 X$, $M =$ Sc, Y, Zr, Hf; $X =$ Al, In, Sn [5]).

Taking the Θ_D and T_c values estimated from the heat capacity analysis the electron-phonon coupling parameter can

be estimated using the inverted McMillan formula [41]:

$$\lambda_{e\text{-}p} = \frac{1.04 + \mu^* \ln\left(\frac{\Theta_D}{1.45 T_c}\right)}{(1 - 0.62\mu^*)\ln\left(\frac{\Theta_D}{1.45 T_c}\right) - 1.04}.$$

Assuming a standard value of the Coulomb pseudopotential parameter $\mu^* = 0.13$ this yields $\lambda_{e\text{-}p} = 0.53$ indicative of a weak electron-phonon coupling.

The jump in the specific heat at the superconducting transition is normalized as $\Delta C_p/\gamma T_c$ for a weak-coupling BCS superconductor, and its expected value is 1.43. For MgPd$_2$Sb we obtained $\frac{\Delta C_p}{\gamma T_c} = 1.2$, indicating a bulk superconducting transition with a possible influence of sample inhomogeneity and suggesting weakly coupled superconductivity.

The results of resistivity measurements at high pressures are shown in Fig. 7. A linear decrease in T_c with applied pressure is observed, with the slope of $\Delta T_c/P = -0.23(2)$ K/GPa. A weaker but comparable pressure dependence was observed previously in HfPd$_2$Al [42], where the decrease of T_c was attributed to the effect of lattice stiffening that reduces the electron-phonon coupling coefficient, which is also likely applicable to MgPd$_2$Sb. The reported values of the pressure
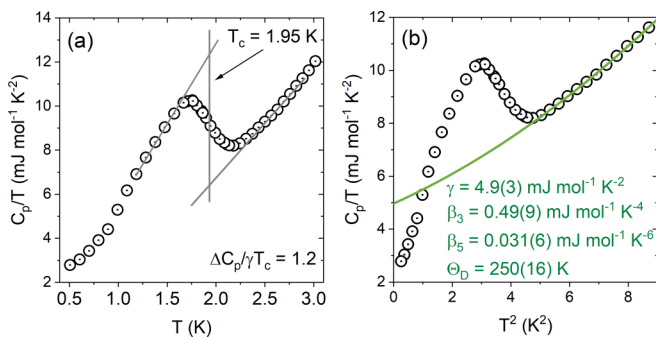

FIG. 6. Low-temperature heat capacity of MgPd$_2$Sb. (a) Equal entropy construction (gray lines) used to estimate the normalized heat capacity jump $\Delta C_p/\gamma T_c = 1.2$. (b) A fit (green line) to the C_p/T vs T^2 data, yielding the γ, β_3, and β_5 electronic and lattice heat capacity coefficients. The Debye temperature calculated from β_3 is $\Theta_D = 250$ K.
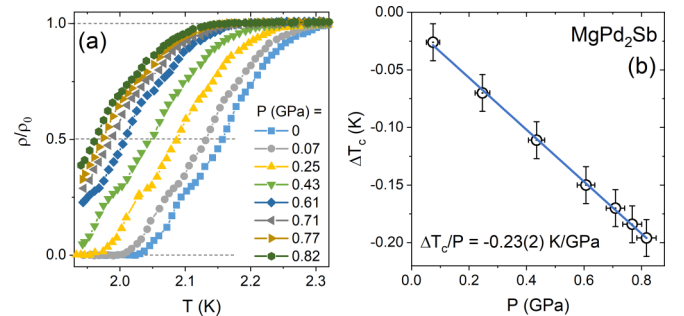

FIG. 7. (a) Plot of temperature-dependent resistivity showing a decrease of T_c with applied pressure. Dashed lines are drawn at ρ_0, $\frac{1}{2}\rho_0$, and 0. (b) The change in T_c (as estimated from the $\frac{1}{2}$ resistivity drop criterion) vs applied pressure. The linear fit (blue line) yields $\Delta T_c/P = -0.23(2)$ K/GPa.
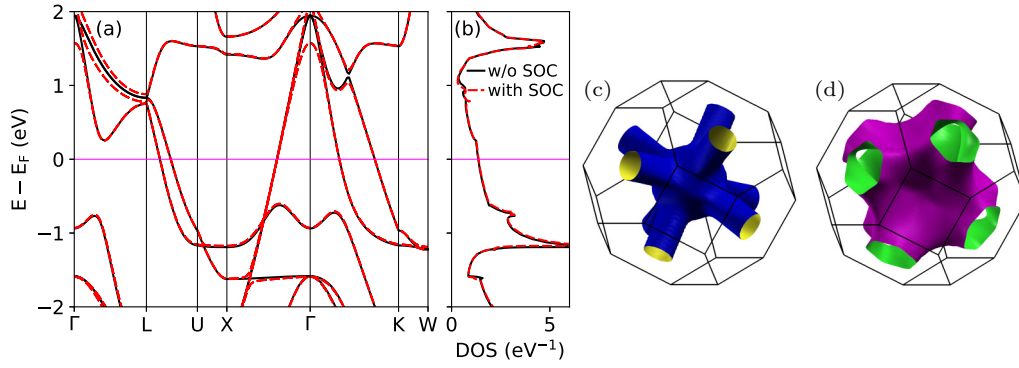
FIG. 8. (a) Electronic band structure and (b) density of states around the Fermi level in MgPd$_2$Sb, calculated with and without spin-orbit coupling; (c), (d) two Fermi surface sheets, plotted with XCRYSDEN [43].

dependence coefficient of T_c for Heusler compounds are gathered in Table I.

IV. THEORETICAL RESULTS

Figure 8 shows the calculated electronic band structure, densities of states (DOS), and Fermi surface of MgPd$_2$Sb. As the constituent atoms of the compound are not particularly heavy, spin-orbit coupling does not visibly influence the electronic states near the Fermi level. Thus further analysis, if not stated otherwise, is based on the scalar-relativistic calculations' results. Two bands cross the Fermi level, which is located on a decreasing slope of the DOS curve, making up two Fermi surface sheets, shown in Figs. 8(c) and 8(d). Total and projected DOS are shown in Fig. 9. The largest contribution to DOS(E_F) comes from Pd 4d and Sb 5p states. Mg contribution to DOS(E_F) is negligible. The DOS shape is dictated by Pd states as DOS of Sb and Mg is approximately constant near E_F. Total DOS(E_F) and band-structure values of the Sommerfeld coefficient γ_{band} are collected in Table III. Comparison with the experimental value of γ via the relation $\gamma_{expt} = \gamma_{band}(1 + \lambda_{e-p})$ yields $\lambda_{e-p} = 0.53$, in agreement with both the value extracted from the McMillan formula and the results of *ab initio* electron-phonon calculations (see below).

Phonon dispersion curves and phonon density of states $F(\omega)$ of MgPd$_2$Sb are shown in Fig. 10. The computed phonon structure is stable, as there are no imaginary frequencies and no soft modes, which occur in many Heusler alloys, as in the recently studied LiPd$_2$Ge [44]. As the spin-orbit coupling had negligible effect on the electronic structure of MgPd$_2$Sb, phonon and electron-phonon calculations were done in a scalar-relativistic approximation. We have, however, computed phonons with SOC for two selected **q** points and

calculations confirmed that phonon frequencies were not influenced by SOC, as shown in Fig. 11.

Phonon branches of the lightest atom, Mg, are well separated from the heavier Pd and Sb vibrations. It is worth noting that Sb branches are inverted with Pd ones: Sb mass $M_{Sb} = 121.76$ u is greater than Pd mass $M_{Pd} = 106.42$ u, but the larger contribution to the lowest acoustic modes is from the lighter Pd atom. Inversion of modes is sometimes proposed to be correlated with the observed dynamical instabilities in some Heusler compounds [45]; however, such a situation is not seen here. Figure 11 shows the phonon dispersion relation with shading proportional to the phonon linewidths γ_{qv} which measure the strength of the electron-phonon coupling [46–48]:

$$\gamma_{qv} = 2\pi \omega_{qv} \sum_{ij} \int \frac{d^3k}{\Omega_{BZ}} |g_{qv}(\mathbf{k}, i, j)|^2 \delta(E_{q,i} - E_F)$$
$$\times \delta(E_{\mathbf{k+q},j} - E_F),$$

$$g_{qv}(\mathbf{k}, i, j) = \sum_s \left(\frac{\hbar}{2M_s\omega_{qv}} \right)^{1/2} \left\langle \psi_{i,\mathbf{k}} \frac{dV_{scf}}{d\hat{u}_{v,s}} \cdot \hat{e}_v \psi_{j,\mathbf{k+q}} \right\rangle.$$

ω_{qv} is the phonon frequency at the **q** vector for the mode v, M_s is the mass of atom s, $\psi_{i,\mathbf{k}}$ is an electron wave function, $\hat{e}_v$ is a polarization vector, and $\frac{dV_{scf}}{d\hat{u}_{v,s}}$ is a change of the electronic potential due to a displacement of the atom s in the direction u.

The relatively largest linewidths are observed for the Mg optic modes. Next, the electron-phonon interaction function $\alpha^2F(\omega)$ (Eliashberg function) is calculated by summing contributions from each phonon branch:

$$\alpha^2F(\omega) = \frac{1}{2\pi N(E_F)} \sum_{qv} \delta(\omega - \omega_{qv}) \frac{\gamma_{qv}}{\hbar \omega_{qv}}.$$

TABLE III. Calculated properties of MgPd$_2$Sb: density of states at Fermi energy DOS (E_F), band-structure value of the Sommerfeld coefficient γ_{band}, electron-phonon coupling parameter λ_{e-p} computed from the Eliashberg function and critical temperature T_c from the Allen-Dynes formula assuming $\mu^* = 0.10$.

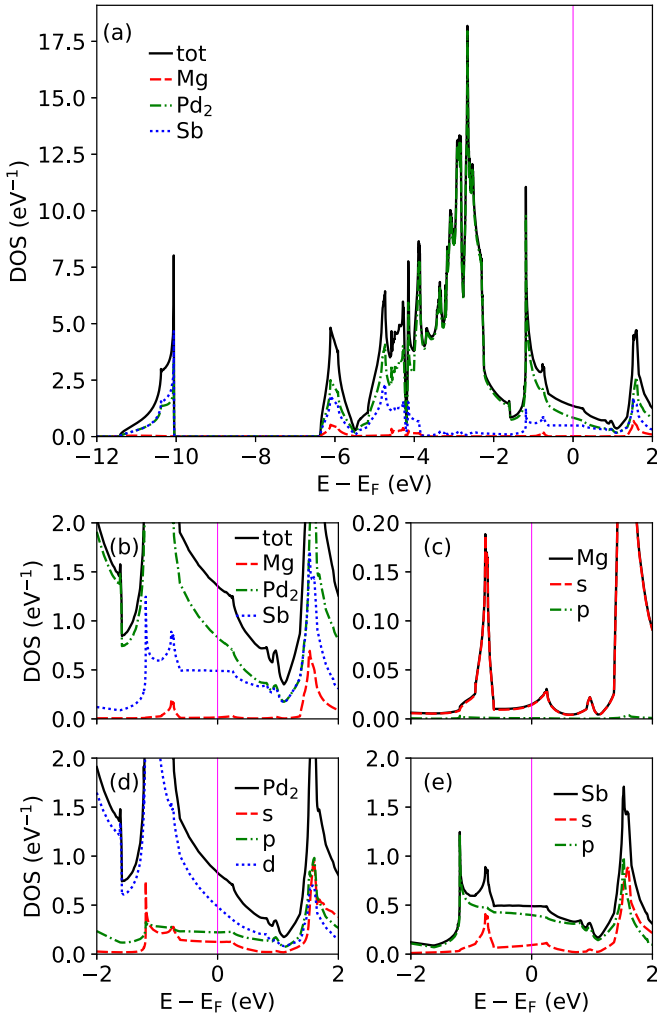|	DOS (E_F)(eV^{-1})	γ_{band} (mJ mol^{-1} K^{-2})	λ_{e-p}	$\langle \omega_{log}^{\alpha^2F} \rangle$ (THz)	T_c (K)
$p = 0$ GPa	1.36	3.20	0.611	1.86	2.16
$p = 1$ GPa	1.34	3.16	0.582	1.93	1.93

FIG. 9. (a) Total and projected DOS of MgPd$_2$Sb; (b) blowup close to the Fermi energy; (c)–(e) DOS projected on atomic orbitals.
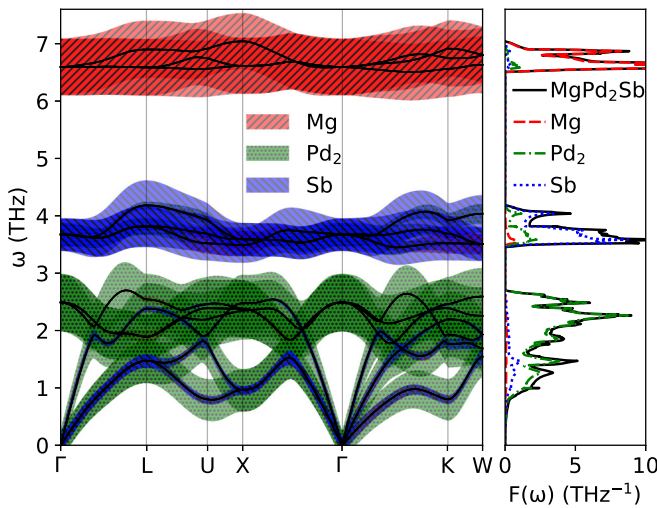

FIG. 10. Phonon dispersion relation and phonon density of states of MgPd$_2$Sb. Color shading with crosshatches represents atomic contributions to phonon branches.
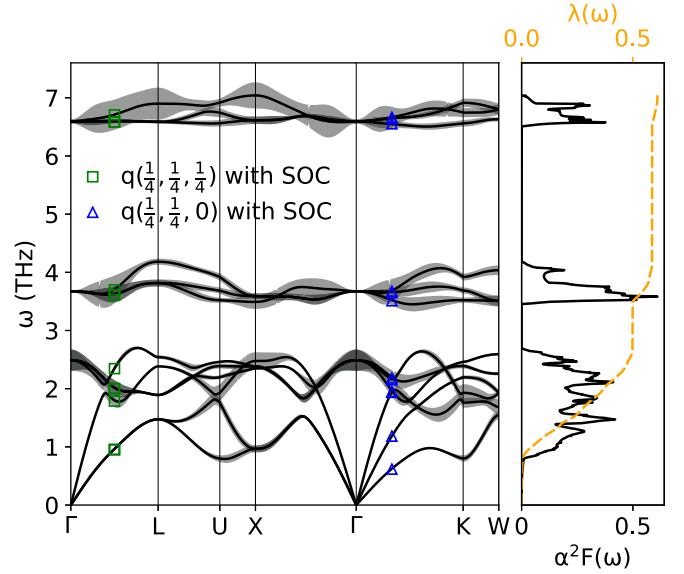

FIG. 11. Left: phonon dispersion relations of MgPd$_2$Sb with shading proportional to phonon linewidths γ_{qv}. Marked points were calculated with SOC. Right: Eliashberg function (solid line) and cumulative electron-phonon coupling constant (dashed line).

The global electron-phonon coupling constant λ is calculated from the Eliashberg function,

$$\lambda_{e\text{-}p} = 2 \int_0^{\omega_{\max}} \frac{\alpha^2 F(\omega)}{\omega} d\omega,$$

and its frequency distribution $\lambda(\omega)$,

$$\lambda(\omega) = 2 \int_0^{\omega} \frac{\alpha^2 F(\omega')}{\omega'} d\omega'$$

is plotted on the top of the $\alpha^2 F(\omega)$ function in Fig. 11. As $\lambda_{e\text{-}p}$ is inversely proportional to ω^2 the largest contribution comes from the low-frequency part of the spectrum. The first six, mainly Pd modes, contribute about 80% to the total $\lambda_{e\text{-}p}$ value, leaving 15% and 5% to Sb- and Mg-dominated branches. Therefore, electron coupling with Pd atoms vibrations is the most important factor in the superconductivity of MgPd$_2$Sb. The computed value of $\lambda_{e\text{-}p} = 0.61$ is close to the values estimated from the McMillan formula and experimental T_c, as well as from the electronic specific heat coefficient γ ($\lambda_{e\text{-}p} = 0.53$ in both cases). The theoretical value of the superconducting critical temperature may be now obtained using the Allen-Dynes formula [45]:

$$T_c = \frac{\langle \omega_{\log}^{\alpha^2 F} \rangle}{1.20} \exp\left[\frac{-1.04(1 + \lambda_{e\text{-}p})}{\lambda_{e\text{-}p} - \mu^*(1 + 0.62\lambda_{e\text{-}p})} \right],$$

$$\langle \omega_{\log}^{\alpha^2 F} \rangle = \exp\left[\int_0^{\omega_{\max}} \alpha^2 F(\omega) \ln(\omega) \frac{d\omega}{\omega} \bigg/ \int_0^{\omega_{\max}} \alpha^2 F(\omega) \frac{d\omega}{\omega} \right].$$

Assuming the Coulomb pseudopotential parameter to be of the typical value of $\mu^* = 0.10$ we arrive at $T_c = 2.16$ K, in agreement with the experimental findings, whereas taking $\mu^* = 0.13$ would result in slightly underestimated $T_c =$
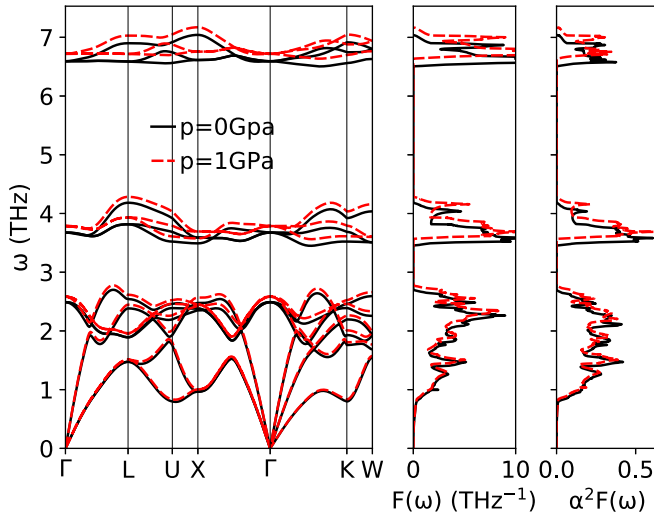
FIG. 12. Effect of pressure on phonon dispersion curves (left panel), phonon density of states F(ω) (middle panel), and Eliashberg function $\alpha^2F(\omega)$ (right panel) in MgPd$_2$Sb.

1.54 K. This overall good agreement clearly shows the electron-phonon origin of superconductivity in MgPd$_2$Sb.

Furthermore, to complete the comparison of the theoretical prediction with experimental works, calculations with applied external pressure of 1 GPa were done. The computed lattice parameter is $a = 6.528$ Å. As this pressure is relatively small, electronic dispersion relations did not change visibly, giving a slightly decreased DOS(E_F) value (see Table III). However, noticeable differences are observed in the phonon spectrum, presented in Fig. 12. Under the external pressure the Heusler structure remains stable and no phonon softening is observed for the acoustic part of the spectrum. Optical phonon branches move upwards, which is a typical sign of lattice stiffening. The comparison of the Eliashberg functions is additionally done in Fig. 12, and the electron-phonon coupling constant λ_{e-p} visibly decreases from 0.61 (0 GPa) to 0.58 (1 GPa). This is followed by the decrease in the superconducting critical temperature, and the computed rate of $\Delta T_c/p \approx -0.23$ K/GPa is again in excellent agreement with the experimental result.

V. CONCLUSIONS

As noted earlier [5,49], most of the known superconductors show the VEC = 27. This was recently rationalized by Kautzsch *et al.* [49] based on rigid band considerations of the electronic structure of Heusler compounds: at a certain electron count VEC $\approx$ 27 the Fermi level lies in the proximity of a Van Hove singularity, resulting in an increased electronic density of states (DOS) and a tendency to either undergo a structural distortion (as in the case of LuPt$_2$In [50]) or superconducting transition. The T_c differences between iso-electronic compounds are then a result of subtle differences in electronic structure, phonon structures, and/or the amount of structural disorder.

Based on electron counting rules and supported by results of high-throughput calculations we have synthesized a previously unreported, Mg-bearing Heusler compound, which, in accordance with the theoretical calculations, was found to be superconducting, with $T_c \approx 2.2$ K. MgPd$_2$Sb is a weakly coupled type-II BCS superconductor.

Table I gathers normal- and superconducting-state parameters for MgPd$_2$Sb and other reported full Heusler superconductors. Compared to other members of this family for which the data are available, MgPd$_2$Sb has a rather low electronic heat capacity coefficient γ and the lowest upper critical field H_{c2}. The electron-phonon coupling coefficient λ_{e-p} is close to that observed in other compounds with similar T_c (ZrPd$_2$In, HfPd$_2$In, YPd$_2$Pb, NbNi$_2$Al, LiGa$_2$Rh), which is consistent with the McMillan formula, as most of the Heusler superconductors have similar Debye temperature on the order of 200 K. The pressure dependence of T_c was found to be second strongest among the reported values after TmPd$_2$Pb.

[1] J. Dshemuchadse and W. Steurer, More statistics on inter-metallic compounds—ternary phases, Acta Crystallogr., Sect. A: Found. Adv. **71**, 335 (2015).

[2] R. Pöttgen and D. Johrendt, *Intermetallics, Synthesis, Structure, Function*, 2nd ed. (De Gruyter, Berlin, 2019).

[3] F. Heusler, Über magnetische Manganlegierungen, Verh. Dtsch. Phys. Ges. **5**, 219 (1903).

[4] J. H. Wernick, G. W. Hull, T. H. Geballe, J. E. Bernardini, and J. V. Waszczak, Superconductivity in ternary Heusler intermetal-lic compounds, Mater. Lett. **2**, 90 (1983).

[5] T. Klimczuk, C. H. Wang, K. Gofryk, F. Ronning, J. Winterlik, G. H. Fecher, J.-C. Griveau, E. Colineau, C. Felser, J. D. Thompson, D. J. Safarik, and R. J. Cava, Superconductivity in the Heusler family of intermetallics, Phys. Rev. B **85**, 174505 (2012).

[6] O. Pavlosiuk, D. Kaczorowski, and P. Wiśniewski, Supercon-ductivity and Shubnikov–de Haas oscillations in the noncen-trosymmetric half-Heusler compound YPtBi, Phys. Rev. B **94**, 035130 (2016).

[7] O. Pavlosiuk, D. Kaczorowski, and P. Wiśniewski, Shubnikov–de Haas oscillations, weak antilocalization effect and large linear magnetoresistance in the putative topological supercon-ductor LuPdBi, Sci. Rep. **5**, 9158 (2015).

[8] J. Winterlik, G. H. Fecher, A. Thomas, and C. Felser, Supercon-ductivity in palladium-based Heusler compounds, Phys. Rev. B **79**, 064508 (2009).

[9] W. Al-Sawai, H. Lin, R. S. Markiewicz, L. A. Wray, Y. Xia, S.-Y. Xu, M. Z. Hasan, and A. Bansil, Topological electronic structure in half-Heusler topological insulators, Phys. Rev. B **82**, 125208 (2010).

[10] Z. K. Liu, L. X. Yang, S.-C. Wu, C. Shekhar, J. Jiang, H. F. Yang, Y. Zhang, S.-K. Mo, Z. Hussain, B. Yan, C. Felser, and Y. L. Chen, Observation of unusual topological surface states in half-Heusler compounds LnPtBi ($Ln =$ Lu, Y), Nat. Commun. **7**, 12924 (2016).

[11] Y. Sun and C. Felser, Topological materials in Heusler compounds, in *Topological Matter, Lectures from the Topological Matter School 2017*, edited by D. Bercioux, J. Cayssol, M.G. Vergniory, and M. Reyes Calvo (Springer International Publishing, Cham, Switzerland, 2018), pp. 199–210.

[12] O. Pavlosiuk, D. Kaczorowski, X. Fabreges, A. Gukasov, and P. Wiśniewski, Antiferromagnetism and superconductivity in the half-Heusler semimetal HoPdBi, Sci. Rep. **6**, 18797 (2016).

[13] P.-J. Guo, H.-C. Yang, K. Liu, and Z.-Y. Lu, Type-II Dirac semimetals in the YPd$_2$Sn class, Phys. Rev. B **95**, 155112 (2017).

[14] X.-Q. Chen, R. Podloucky, and P. Rogl, *Ab initio* prediction of half-metallic properties for the ferromagnetic Heusler alloys Co$_2$$M$Si ($M =$ Ti, V, Cr), J. Appl. Phys. **100**, 113901 (2006).

[15] N. I. Kourov, V. V. Marchenkov, A. V. Korolev, L. A. Stashkova, S. M. Emel'yanova, and H. W. Weber, Specific features of the properties of half-metallic ferromagnetic Heusler alloys Fe$_2$MnAl, Fe$_2$MnSi, and Co$_2$MnAl, Phys. Solid State **57**, 700 (2015).

[16] R. Shan, H. Sukegawa, W. H. Wang, M. Kodzuka, T. Furubayashi, T. Ohkubo, S. Mitani, K. Inomata, and K. Hono, Demonstration of Half-Metallicity in Fermi-Level-Tuned Heusler Alloy Co$_2$FeAl$_{0.5}$Si$_{0.5}$ at Room Temperature, Phys. Rev. Lett. **102**, 246601 (2009).

[17] C. Felser, L. Wollmann, S. Chadov, G. H. Fecher, and S. S. P. Parkin, Basics and prospective of magnetic Heusler compounds, APL Mater. **3**, 041518 (2015).

[18] T. Graf, S. S. P. Parkin, and C. Felser, Heusler compounds—A material class with exceptional properties, IEEE Trans. Magn. **47**, 367 (2011).

[19] L. Wollmann, A. K. Nayak, S. S. P. Parkin, and C. Felser, Heusler 4.0: Tunable materials, Annu. Rev. Mater. Res. **47**, 247 (2017).

[20] V. Alijani, J. Winterlik, G. H. Fecher, and C. Felser, Tuning the magnetism of the Heusler alloys Mn$_{3-x}$Co$_x$Ga from soft and half-metallic to hard-magnetic for spin-transfer torque applications, Appl. Phys. Lett. **99**, 222510 (2011).

[21] T. Graf, C. Felser, and S. S. P. Parkin, Simple rules for the understanding of Heusler compounds, Prog. Solid State Chem. **39**, 1 (2011).

[22] N. Fukatani, K. Ueda, and H. Asano, Epitaxial strain and antiferromagnetism in Heusler Fe$_2$VSi thin films, J. Appl. Phys. **109**, 073911 (2011).

[23] X. T. Wang, Z. X. Cheng, J. L. Wang, H. Rozale, L. Y. Wang, Z. Y. Yu, J. T. Yang, and G. D. Liu, Strain-induced diverse transitions in physical nature in the newly designed inverse Heusler alloy Zr$_2$MnAl, J. Alloys Compd. **686**, 549 (2016).

[24] M. Belmeguenai, F. Zighem, G. Woltersdorf, Y. Roussigné, S. M. Chérif, K. Westerholt, and G. Bayreuther, Anisotropy and dynamic properties of Co$_2$MnGe Heusler thin films, J. Magn. Magn. Mater. **321**, 750 (2009).

[25] V. V. Khovaylo, V. V. Rodionova, S. N. Shevyrtalov, and V. Novosad, Magnetocaloric effect in "reduced" dimensions: Thin

films, ribbons, and microwires of Heusler alloys and related compounds, Phys. Status Solidi B **251**, 2104 (2014).

[26] T. Graf, F. Casper, J. Winterlik, B. Balke, G. H. Fecher, and C. Felser, Crystal structure of new Heusler compounds, Z. Anorg. Allg. Chem. **635**, 976 (2009).

[27] K. Persson, *Materials Project*, Materials data on MgSbPd$_2$ (SG:225) (2016), http://dx.doi.org/10.17188/1315794.

[28] A. Jain, S. P. Ong, G. Hautier, W. Chen, W. D. Richards, S. Dacek, S. Cholia, D. Gunter, D. Skinner, and G. Ceder, Commentary: The Materials Project: A materials genome approach to accelerating materials innovation, APL Mater. **1**, 011002 (2013).

[29] J. E. Saal, S. Kirklin, M. Aykol, B. Meredig, and C. Wolverton, Materials design and discovery with high-throughput density functional theory: The open quantum materials database (OQMD), JOM **65**, 1501 (2013).

[30] S. Kirklin, J. E. Saal, B. Meredig, A. Thompson, J. W. Doak, M. Aykol, S. Rühl, and C. Wolverton, The open quantum materials database (OQMD): Assessing the accuracy of DFT formation energies, npj Comput. Mater. **1**, 15010 (2015).

[31] T. Klimczuk, Q. Xu, E. Morosan, J. D. Thompson, H. W. Zandbergen, and R. J. Cava, Superconductivity in noncentrosymmetric Mg$_{10}$Ir$_{19}$B$_{16}$, Phys. Rev. B **74**, 220502(R) (2006).

[32] T. G. Amos, Q. Huang, J. W. Lynn, T. He, and R. J. Cava, Carbon concentration dependence of the superconducting transition temperature and structure of MgC$_x$Ni$_3$, Solid State Commun. **121**, 73 (2002).

[33] J. Rodríguez-Carvajal, Recent advances in magnetic structure determination by neutron powder diffraction, Phys. B (Amsterdam, Neth.) **192**, 55 (1993).

[34] P. Giannozzi, S. Baroni, N. Bonini, M. Calandra, R. Car, C. Cavazzoni, D. Ceresoli, G. L. Chiarotti, M. Cococcioni, I. Dabo, A. D. Corso, S. de Gironcoli, S. Fabris, G. Fratesi, R. Gebauer, U. Gerstmann, C. Gougoussis, A. Kokalj, M. Lazzeri, L. Martin-Samos *et al.*, QUANTUM ESPRESSO: A modular and open-source software project for quantum simulations of materials, J. Phys.: Condens. Matter. **21**, 395502 (2009).

[35] P. Giannozzi, O. Andreussi, T. Brumme, O. Bunau, M. B. Nardelli, M. Calandra, R. Car, C. Cavazzoni, D. Ceresoli, M. Cococcioni, N. Colonna, I. Carnimeo, A. D. Corso, S. de Gironcoli, P. Delugas, R. A. DiStasio, A. Ferretti, A. Floris, G. Fratesi, G. Fugallo *et al.*, Advanced capabilities for materials modelling with QUANTUM ESPRESSO, J. Phys.: Condens. Matter. **29**, 465901 (2017).

[36] A. Dal Corso, Pseudopotentials periodic table: From H to Pu, Comput. Mater. Sci. **95**, 337 (2014).

[37] J. P. Perdew, K. Burke, and M. Ernzerhof, Generalized Gradient Approximation Made Simple, Phys. Rev. Lett. **77**, 3865 (1996).

[38] S. Baroni, S. de Gironcoli, A. Dal Corso, and P. Giannozzi, Phonons and related crystal properties from density-functional perturbation theory, Rev. Mod. Phys. **73**, 515 (2001).

[39] N. R. Werthamer, E. Helfand, and P. C. Hohenberg, Temperature and purity dependence of the superconducting critical field, H_{c2}. III. Electron spin and spin-orbit effects, Phys. Rev. **147**, 295 (1966).

[40] E. Helfand and N. R. Werthamer, Temperature and purity dependence of the superconducting critical field, H_{c2}. II, Phys. Rev. **147**, 288 (1966).

[41] W. L. McMillan, Transition temperature of strong-coupled superconductors, Phys. Rev. **167**, 331 (1968).

[42] B. Wiendlocha, M. J. Winiarski, M. Muras, C. Zvoriste-Walters, J.-C. Griveau, S. Heathman, M. Gazda, and T. Klimczuk, Pressure effects on the superconductivity of the $HfPd_2Al$ Heusler compound: Experimental and theoretical study, Phys. Rev. B **91**, 024509 (2015).

[43] A. Kokalj, XCRYSDEN—a new program for displaying crystalline structures and electron densities, J. Mol. Graphics Modell. **17**, 176 (1999).

[44] K. Górnicka, G. Kuderowicz, E. M. Carnicom, K. Kutorasiński, B. Wiendlocha, R. J. Cava, and T. Klimczuk, Soft-mode enhanced type-I superconductivity in $LiPd_2Ge$, Phys. Rev. B **102**, 024507 (2020).

[45] A. T. Zayak, P. Entel, K. M. Rabe, W. A. Adeagbo, and M. Acet, Anomalous vibrational effects in nonmagnetic and magnetic heusler alloys, Phys. Rev. B **72**, 054113 (2005).

[46] M. Wierzbowska, S. de Gironcoli, and P. Giannozzi, Origins of low-and high-pressure discontinuities of T_c in niobium, arXiv:cond-mat/0504077.

[47] R. Heid, K.-P. Bohnen, I. Y. Sklyadneva, and E. V. Chulkov, Effect of spin-orbit coupling on the electron-phonon interaction of the superconductors Pb and Tl, Phys. Rev. B **81**, 174527 (2010).

[48] S. Gołąb and B. Wiendlocha, Electron-phonon superconductivity in $CaBi_2$ and the role of spin-orbit interaction, Phys. Rev. B **99**, 104520 (2019).

[49] L. Kautzsch, F. Mende, G. H. Fecher, J. Winterlik, and C. Felser, Are AuPdTM (T = Sc, Y and M = Al, Ga, In), Heusler compounds superconductors without inversion symmetry? Materials **12**, 2580 (2019).

[50] T. Gruner, D. Jang, Z. Huesges, R. Cardoso-Gil, G. H. Fecher, M. M. Koza, O. Stockert, A. P. Mackenzie, M. Brando, and C. Geibel, Charge density wave quantum critical point with strong enhancement of superconductivity, Nat. Phys. **13**, 967 (2017).

[51] M. J. Johnson and R. N. Shelton, Pressure effects on the superconductivity of ternary rare earth palladium Heusler alloys, Solid State Commun. **52**, 839 (1984).

[52] E. M. Carnicom, W. Xie, Z. Yang, K. Górnicka, T. Kong, T. Klimczuk, and R. J. Cava, Importance of specific heat characterization when reporting new superconductors: An example of superconductivity in $LiGa_2Rh$, Chem. Mater. **31**, 2164 (2019).

[53] M. J. Johnson, Superconductivity in ternary rare earth palladium Heusler compounds, M.S. thesis, Iowa State University, 1984, available online at https://lib.dr.iastate.edu/rtd/18319.

[54] Y. Aoki, H. R. Sato, T. D. Matsuda, H. Sugawara, and H. Sato, Coexistence of, and competition between, superconductivity and magnetism in $YbPd_2Sn$, J. Magn. Magn. Mater. **177-181**, 559 (1998).

[55] F. S. da Rocha, G. L. F. Fraga, D. E. Brandão, C. M. da Silva, and A. A. Gomes, Specific heat and electronic structure of Heusler compounds Ni_2TAl (T = Ti, Zr, Hf, V, Nb, Ta), Phys. B (Amsterdam, Neth.) **269**, 154 (1999).

[56] J. Winterlik, G. H. Fecher, C. Felser, M. Jourdan, K. Grube, F. Hardy, H. von Löhneysen, K. L. Holman, and R. J. Cava, Ni-based superconductor: Heusler compound $ZrNi_2Ga$, Phys. Rev. B **78**, 184506 (2008).

[57] C. Benndorf, O. Niehaus, H. Eckert, and O. Janka, ^{27}Al and ^{45}Sc NMR Spectroscopy on ScT$_2$Al and Sc($T_{0.5}T'_{0.5}$)$_2$Al (T = T' = Ni, Pd, Pt, Cu, Ag, Au) Heusler phases and superconductivity in Sc($Pd_{0.5}Au_{0.5}$)$_2$Al, Z. Anorg. Allg. Chem. **641**, 168 (2015).

[58] S. Waki, Y. Yamaguchi, and K. Mitsugi, Superconductivity of Ni_2NbX (X = Al, Ga and Sn), J. Phys. Soc. Jpn. **54**, 1673 (1985).